Supplementary Information

Broadband room temperature strong coupling between quantum dots and metamaterials.

Chaitanya Indukuri [1], Ravindra Kumar Yadav [1] and J. K. Basu [1] *

1) *Department of Physics, Indian Institute of Science, Bangalore, 560 012, India*

* basu@physics.iisc.ernet.in

The main manuscript dealt about the emergence of strong interaction between hyperbolic metamaterials and QE are discussed. In this supplementary information we will describe the experimental method to prepare hyperbolic template and QD transfer on to the template and there characterization by FESEM and AFM imaging, as well as details of time resolved data analysis and FDTD simulation.

1) Preparation of HMM:

In our experiment, porous alumina (Al_2O_3) template is fabricated from bulk aluminum sheet purchased from the Alfa Aesar. The pore diameter and inter pore distance are controlled by anodization condition. Deep pores make these templates very useful for making nano structures with very high aspect ratio. Before anodization, the aluminum foil is electropolished to remove oil and organic contaminations and to reduce the surface roughness. In oxalic acid solution, the porous alumina grows gradually by anodizing aluminum under the electric field. Pore diameter and inter pore distance depends on the electrolyte solutions and applied voltage. In our work, oxalic acid and two different voltages 40 V and 50 V are used for fabrication of Al_2O_3 template with different pore radius and inter pore distance. Long first anodization improves the pore regularity, so we did first anodization for 14 hr. Since this process initiates pores at random positions in first anodization, pores are located very random with large size distribution. By removing 1st anodization oxide layer, it results in crests and troughs on the Al surface that acts as a self-assembled template for 2nd anodization. In case of second anodization, ordering of pores increases for the same parameters of the first anodization. The thickness of the membrane is controlled at the time of second anodization. CuCl2 solution was used to remove the Al layer. For removing Al_20_3 barrier layer membrane is dipped in 6 wt % H3PO4 solution at 30^0 C for 20 min resulting in a through hole alumina membrane. The barrier layer formed after second anodization is removed and 20-30 nm Au deposited on top of the template by RF sputtering method. After Au deposition on one side of the template silver nanowires were grown for 2 h within the nanopores via electrochemical deposition using an electrolyte mixture of AgBr=0.1 M, $Na_2S_2O_3$=0.25 M, and Na_2SO_3 = 0.2 M at a constant voltage of -0.7 V versus a saturated $Hg/HgSO_4$-electrode [Ref: **1**].

After electrodeposition of Ag nano-wire, for optical measurements we removed bottom sputtered Au layer of thickness 30 nm by using FIB. The time taken for removing Au coating is around 45 min. All the FESEM images shown in the figure were taken from the etched regions by FIB. Small ion currents were used for reduce the roughness of the etched region. The areas etched are 200 μm x 200μm which can be identified by optical microscopy with white light illumination.

All the optical measurements reported in this letter were collected in these etched regions. After etching, these templates were transferred on to the glass substrate and spin coated with polymer films with a speed of 1000 rpm for 60 sec to form uniform spacer layers of controlled thickness. The spacer layer thickness was controlled by varying the concentration of polymer solution.

Both SCdSe (5 nm) and LCdSe (6.5 nm) were synthesized by method described in **Ref:2**. The following chemical are used for synthesis of Trioctylphosphine oxide (TOPO) capped CdSe QDs: CdO powder, TOPO, Se powder, Trioctylphosphine (TOP) from sigma-Aldrich and used without any further purification and methanol from Merck (Germany). CdO powder 6.6 mg with 1.85 g TOPO and 40 mg HPA were added in three neck flask and heated at 300^0c for 1 hr under constant nitrogen N_2 flow. HPA completely dissolves and turns to a transparent solution. The stock solution of completely dissolved Se powder in TOP is added at same temperature and kept for 5 min. Size of the QDs is controlled by temperature and time of the reaction. After reaching room temperature, methanol is added to reaction flask to extract CdSe QDs. A reddish powder of CdSe precipitates after several hours. This precipitate is collected and cleaned with mixture of toluene and methanol for several times to remove excess TOPO present in the CdSe QD powder. The final QD's were dispersed in chloroform or toluene depending up on experimental requirement. All the CdSe quantum dots were transferred on to the HMM template at identical surface density of QDs (and surface pressure) using the well-known Langmuir-Blodgett technique. By achieving desirable area density of QD's the monolayer formed on the water surface will transferred to any substrate. By keeping the concentration of solution and trough area same, we can attain very high degree of reproducibility in different films [Ref: **3,4**]. From the Fig S1 it is clear that all the samples were transferred at same number density of QD's per area. We can control both number QD's per area and distance between the QD's. In our experiment all parameters of CdSe monolayer were same (both number of particles and inter particle distance).

Calculation of Number density of QDs:

Concentration of CdSe has taken 0.7mg/ml. We spread 0.55 ml CdSe solution in to $45cm^2$ trough area which leads 35 mN/m trough pressure as shown in isotherm Figure S1. Density of CdSe has taken $5.816g/cm^3$(as bulk). Number density of CdSe is calculated using following relation:

$$n = \frac{3.c.V}{4.\pi.r^3.\rho_{CdSe}.A} \qquad (1)$$

Where c = conc. Of CdSe, V= Volume of CdSe solution, ρ_{CdSe} = density of QD, r = radius of CdSe, A =Trough Area in which CdSe spread.

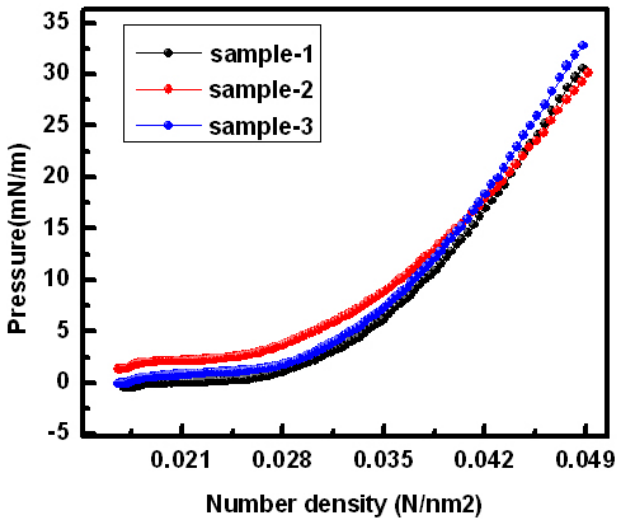

Figure S1: Surface pressure as a function of number density of QD's per (nm^{-2}) transferred on to the HMM template surface. Figure shows the all the samples were transferred at same number density.

From equation (1) we have calculated number of QD per unit cell area (***N***) for *f*=0.15 and 0.2 HMM templates which are ~ 570 and ~ 350 respectively for the cases of closed packed QD monolayers.

Atomic force microscopy:

Atomic force microscopy measurements (NT-MDT–NTEGRA model AFM) were performed using Non-contact mode.

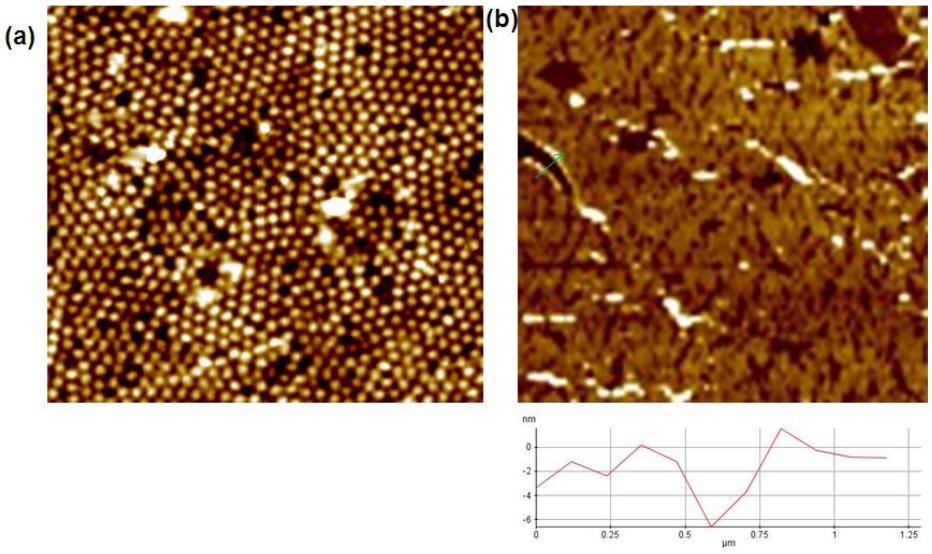

Figure S2: shows the **(a)** AFM of top surface of the *f*=0.15 HMM template. **(b)** AFM image of CdSe monolayer on top of the *f*= 0.15 HMM template.

Scanning electron microscopy images:

Ultra high resolution scanning electron imaging was taken using The ULTRA 55 FESEM. 5 kV voltage and InLens detector is used for imaging.

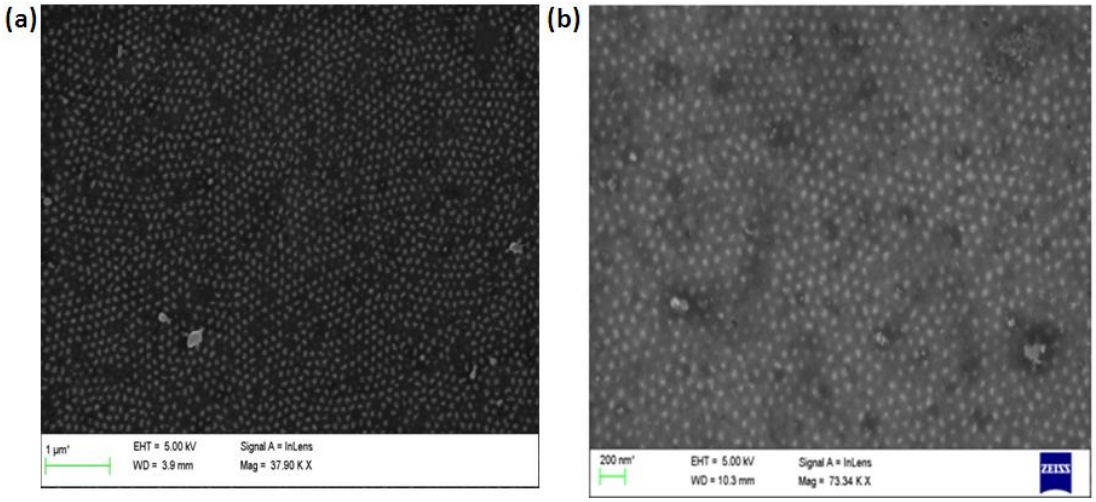

Figure S3: Shows the FESEM image of the top surface of HMM with **(a)** *f*=0.15, **(b)** *f*= 0.2.

2) Experimental setup for steady state PL measurements:

All the steady state PL measurements were performed on reflection mode geometry as shown in figure S4. 488 blue line from Ar-ion laser focused on to the sample using 20X objective and emission was collected through the same objective. The signal is transferred to spectrograph through the fiber coupler.

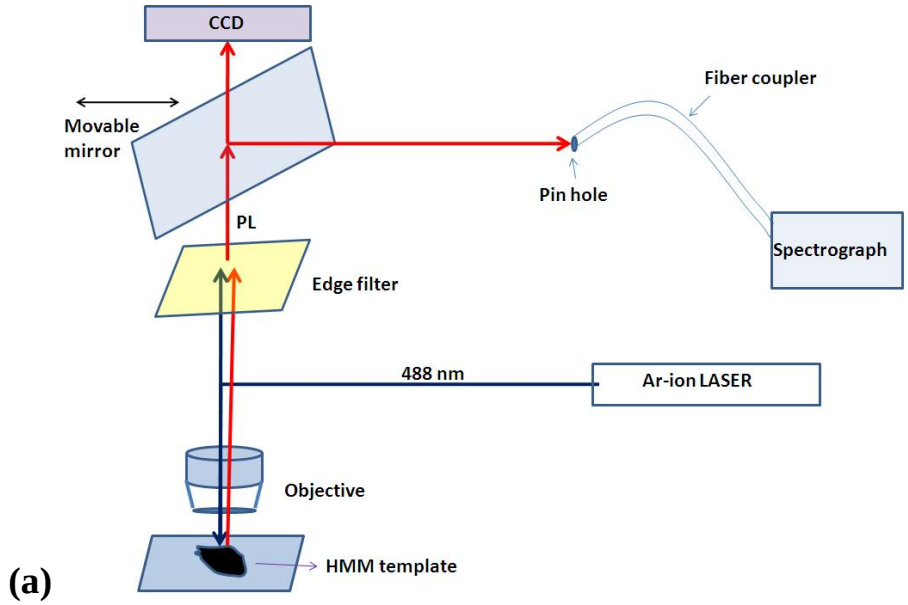

(a)

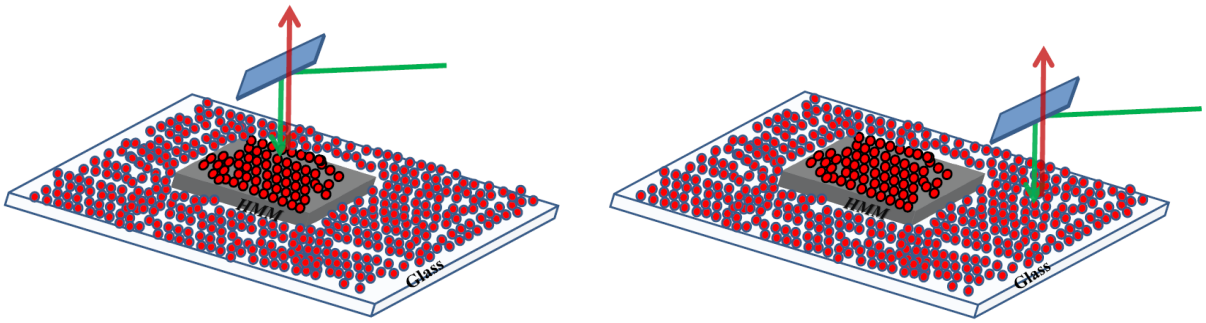

(b) (c)

Figure S4: (a) Shows a schematic diagram of experimental setup. 488 nm excitation line from Ar-ion LASER is focused on to the HMM template and the emission is collected through same objective. The PL signal is directed to the CCD or pin hole connected to spectrograph through fiber by placing the movable mirror in the beam path. (b) and (c) shows the PL measurement from HMM template and adjacent glass by moving sample stage. Green arrow shows the laser while rad line shows the PL emission.

(3) "*h*" dependent PL spectra of LCdSe:

In this section we have shown h dependent steady state PL spectra of LCdSe QD on HMM.

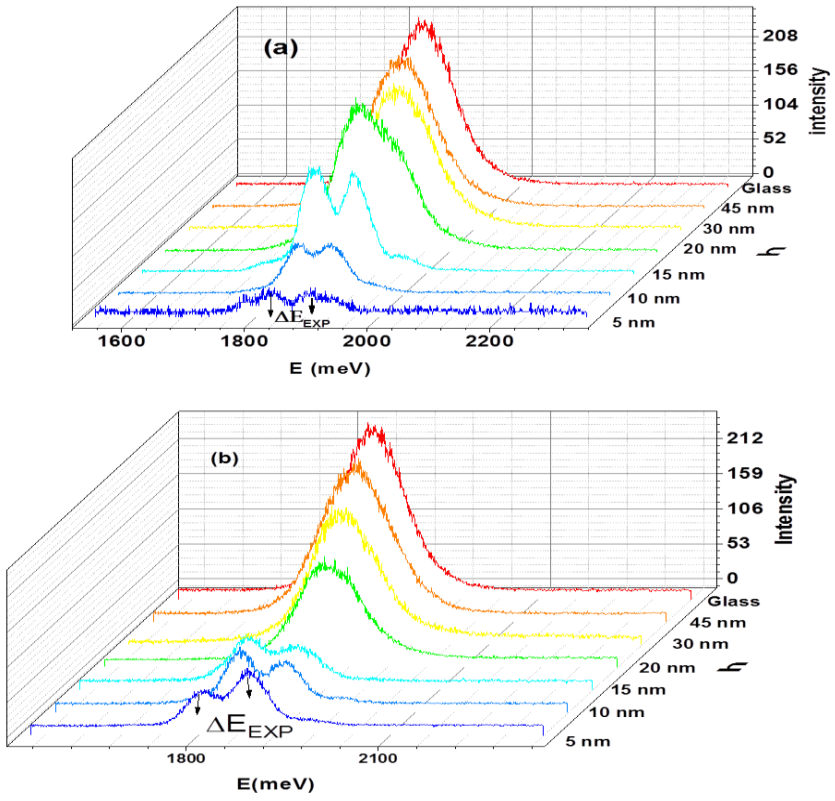

Figure S5: PL measurements on LCdSe monolayers on HMM template with **(a)** *f* = 0.15 and **(b)** *f*=0.2, as well as on glass.

(4) Method of calculating the splitting $\Delta E_{exp}(h)$:

To calculate the PL intensity splitting, we fitted with all PL spectra with double Gaussians and the difference in peak positions were taken as splitting ΔE_{exp}. The PL spectra shown in the

figure for *f*=0.20 HMM and same type of fitting were also done in case of *f*=0.15 HMM template and for LCdSe QD samples also. Figure S6 shows the typical spectra of PL splitting and we fitted different splitting spectra for same spacer thickness and taken average over multiple spectra.

$$\Delta E_{exp}(h) = | E_{+} - E_{-} | \qquad (2)$$

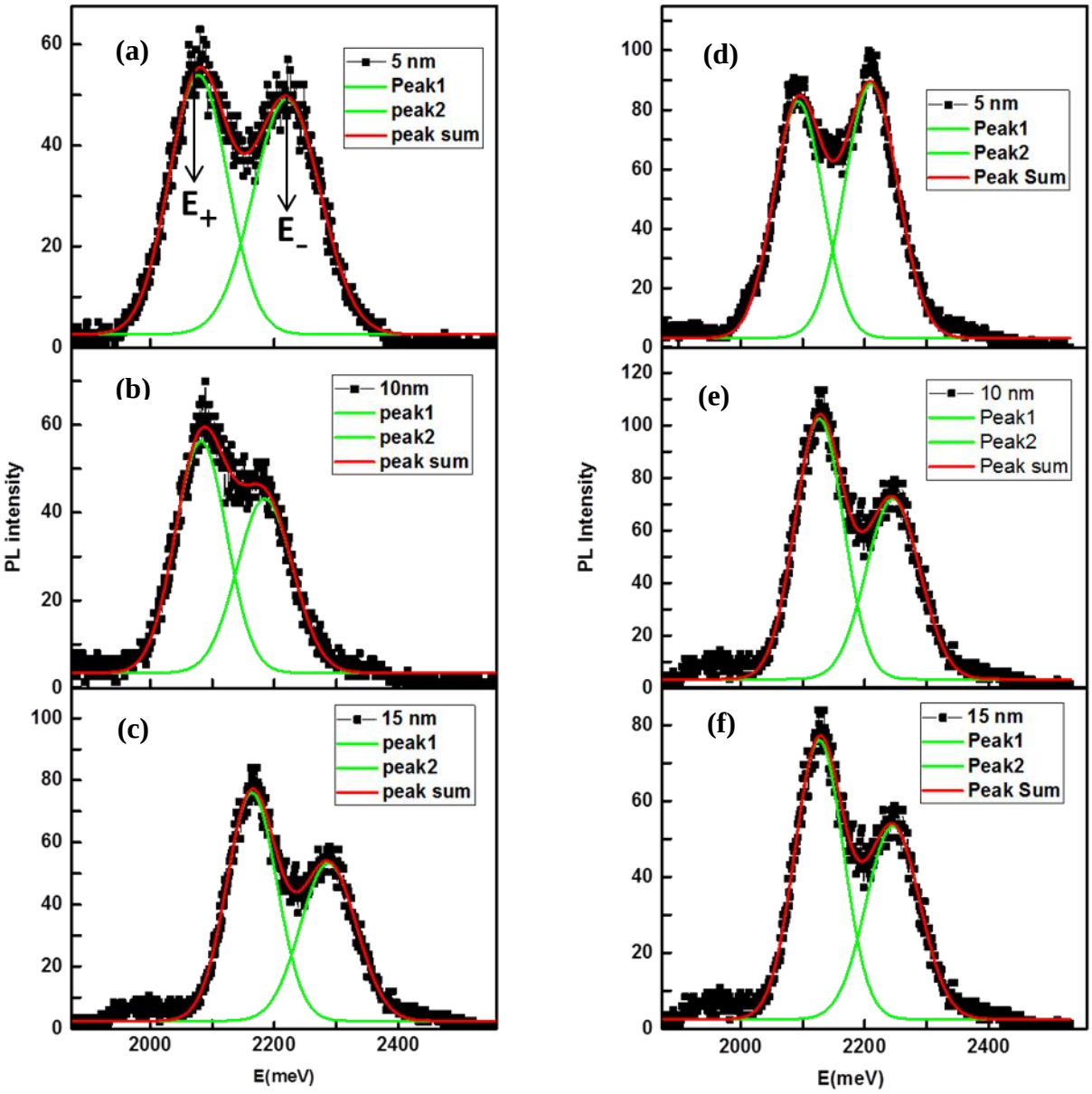

Figure S6: PL spectra of SCdSe QD monolayers on f= 0.15 HMM template with spacer thickness **(a)** *h*=5nm, **(b)** h=10nm, **(c)** *h*=15nm, and on *f*=0.2 template with spacer thickness **(d)**

h=5, **(e)** *h*=10nm, **(f)** *h*=15nm . The methodology used to extract ΔE_{exp} from the PL spectra using double Gaussian to fit the data as shown in the figure.

(5) Finite difference time domain (FDTD) simulations:

To understand the experimental results we performed the FDTD numerical simulations on the HMM templates and we considered QDs as dipole which emission matches with the QD PL emission spectra.

(a) Method of calculating *S (ω)* Spectral density function:

Now we concentrate on the emission spectra at far field due to strong coupling between QD layer and HMM template. To do this we calculated emission spectra as a function of spacer layer thickness for both the templates (EMT and extended unit cell). The general procedure for calculating *S* (ω) is independent of the template used.

The dipoles were taken such that emission matches with the PL emission of the QD's. For calculating *S (ω)* we have used both local and non-local LDOS by keeping the detector position at dipole and 1 μm away from dipole respectively.

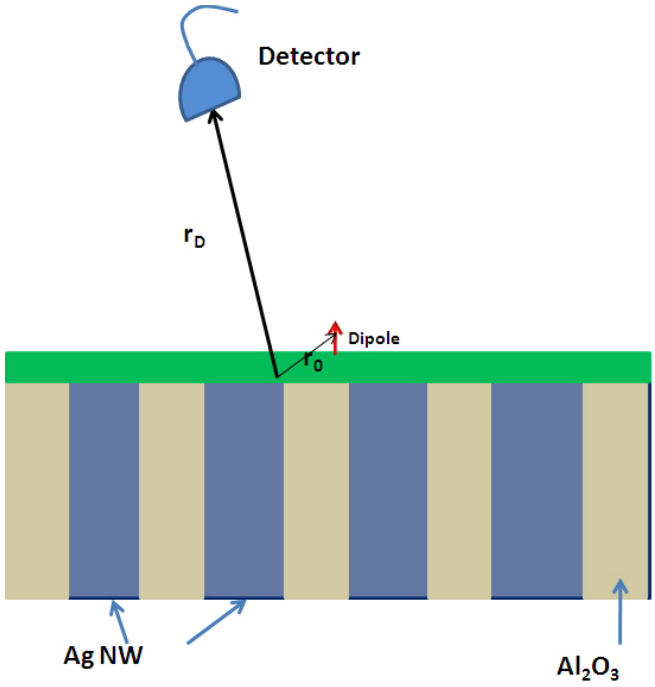

Figure S7: Schematic diagram depicting geometry used for calculating $G(r_D,r_0,\omega)$ and $S(\omega)$.

$S(w)$ is calculated at the far field by using $G(r_D,r_0,\omega)$ function. $G(r_D,r_0,\omega)$ is calculated at detector position about 1 μm distance from the surface of the HMM template. From non-local Green's function was calculated using following relations. **[5,6].**

In general S(w) is defined as

$$S(\omega) = \int_0^\infty dt_2 \int_0^\infty dt1 * e^{-i\omega t} < E(r,t).E^*(r,t) > \quad (3)$$

This can be written as (Taking Fourier Transform).

$$S(w) = < E(r,\omega).E^*(r,\omega) > \quad (4)$$

For single dipole

$$S(\omega) = \left| \frac{\mu.G(r_D,r_o,\omega)(\omega_0+\omega_{PL})}{\omega_{PL}^2-\omega^2-i\omega\gamma_{pl}-2.\omega_{PL}.G(r_0,r_o,\omega).\mu/(h\varepsilon_0)} \right|^2 \quad (5)$$

In case of Multiple QDs above equation can be written as

$$S(\omega)^n = \left| \frac{\mu.\ \sum_n G(r_D,r_o,\omega)\ (\omega_0+\omega_{PL})}{\omega_{PL}^2-\omega^2-i\omega\gamma_{pl}-2.\omega_{PL}.G(r_0,r_o,\omega).\mu/(h\varepsilon_0)} \right|^2 \quad (6)$$

For distance dependence of $S(\omega)$, we calculated different dipole positions from the surface of the template. Here $G(r_D, r_0, \omega)$ non local Green's function, r_D is the position of the monitor, r_0 is the dipole position and μ is dipole moment and ω_{PL} is dipole emission frequency which corresponds to respective QD emission. Summation is over all the dipoles in the unit cell. We have observed the $S(\omega)$ is same for both the templates (EMT and extended unit cell) indicates we can approximate the HMM template as EMT for all the calculations.

FDTD Simulation templates:

FDTD Simulations were performed with both effective medium theory (EMT) and extended cell (6 unit cells of corresponding HMM).

(i) Effective medium theory:

The computational simulation is done by using FDTD with PML boundary condition. In case of EMT calculations effective medium parameters were calculated using Maxwell-Garnet theory and resultant EMT parameters were placed in the diagonal terms of the dielectric tensor. The simulations are run with mesh size 2 nm to find electric field intensity.

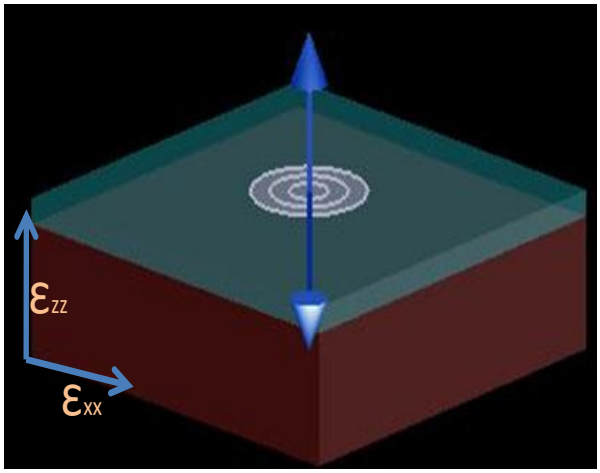

Figure S8: Schematic diagram of EMT layer used to represent the HMM template in FDTD simulation to calculate both $S(\omega)$ and LDOS.

In simulation, two types of templates are used for filling fraction (f) (0.2 and 0.15) of Ag nanowire in Al_2O_3 matrix as used in experiment. Effective medium dielectric constants were taken for the simulations.

The effective medium dielectric constants defined as [Ref: 5].

$$\epsilon_{xx} = \epsilon_{yy} = \frac{(1+f)\epsilon_m.\ \epsilon_d + (1-f)\epsilon_m.\ \epsilon_d}{(1-f)\epsilon_m + (1+f)\epsilon_d} \quad (7)$$

$$\epsilon_{zz} = (f)\epsilon_m + (1-f)\epsilon_d \quad (8)$$

Where ϵ_{xx} , ϵ_{yy} and ϵ_{zz} are diagonal terms of dielectric tensor and ϵ_m and ϵ_d are the dielectric dielectric constants of Ag and Al_2O_3 matrix respectively. The values of silver were taken from Johnson and Christy [7] whereas Al_2O_3 dielectric constant was taken as 2.56 and independent of wavelength.

Figure S9 shows the dispersion relation for different diagonal components of the permittivity tensor which shows the negative values for some frequency range which show the behavior of HMM in this region. The cut-off frequency where a photonic topological transition occurs depends on *f*.

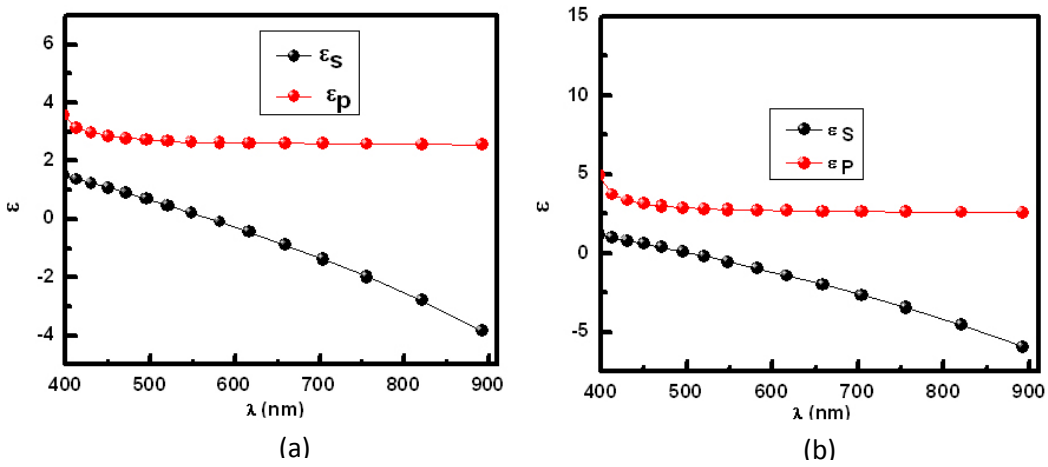

Figure S9: Polarization dependent "dielectric constants" as a function of wavelength for HMM template with (a) *f*=0.15, (b) *f*=0.2 is calculated using EMT and used in the simulations.

(ii) Single wire template: To understand the effect of the internal structure of the HMM template we studied a single nano wire template. Single nano wire template is single Ag nano wire inside the uniform Al_2O_3 matrix.

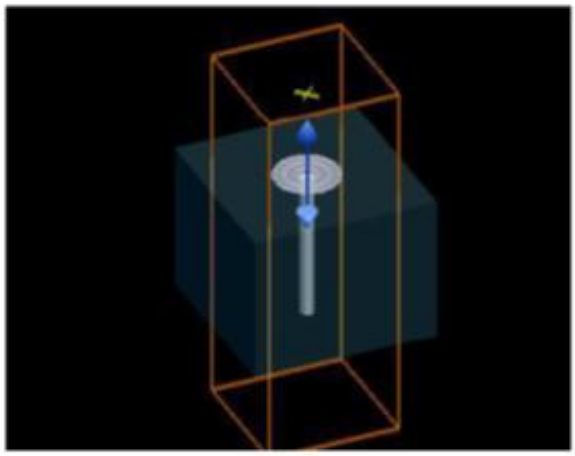

Figure S10: (a) Schematic diagram of single dipole with single Ag nano wire in Al_2O_3**.**

(iii) Extended Unit cell: We have considered hexagonal arrays of Ag nano wires in the Uniform Al_2O_3 matrix. The dielectric constant of the Ag has taken from Johnson and Christy. The dielectric constant of the Al_2O_3 is around 2.56. In case of extended Unit cell we have taken up to six unit cell of the meta atoms in the HMM template as shown in the schematic diagram (Fig **S11**).

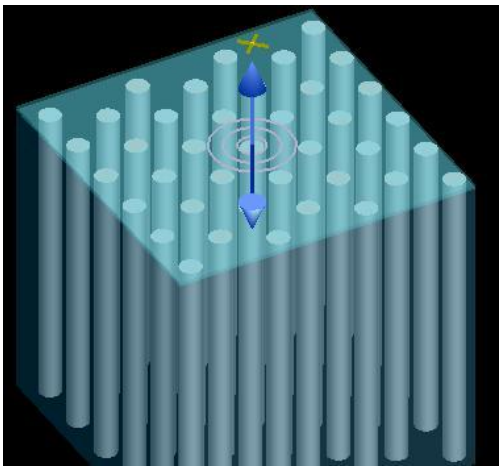

Figure S11: Schematic diagram of extended unit cell template used to represent the HMM template in FDTD simulation to calculate S(ω).

(b) Effect of templates on S(ω):

To obtain further insight we performed exactly same calculations of *S* (ω) but using a single silver nanowire with alumina as background, a unit cell and extended unit cell of silver-alumina template as shown in **Figure S11**. As seen in the **figure S11,** the single nano wire in the uniform Al_2O_3 matrix not showing any splitting in the *S(ω)* , where as if we consider unit cell or extended unit cell we see the clear splitting in the *S(ω)* indicates this effect is coming from the meta-atom (unit cell of the HMM template) but not from the plasmonic effect of the single Ag nano wires in Al_2O_3 matrix.

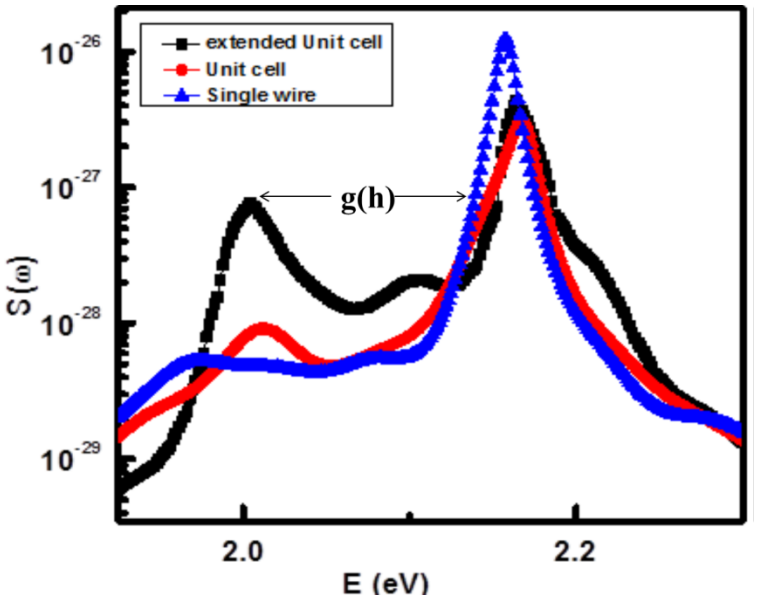

Figure S12: *S*(ω) from coupled dipoles near different type of FDTD templates.

(c) Effect of *N* (Coherent effect):

To see the effect of QD number density we have calculated the S(w) for different number of dipoles per unit cell. We observed the splitting in S(w) is proportional to the square root of the Number density *N*, which is in very good agreement with the experimental observations in the strong coupling region. We have not observed any splitting with single dipole in any of the templates, indicating that the coherent (super-radiant) coupling between QD's, mediated by the large ρ of the HMMs, is responsible for the observed splitting in the *S*(ω) as experimental PL spectra shown in **Figure S5** and **S6**.

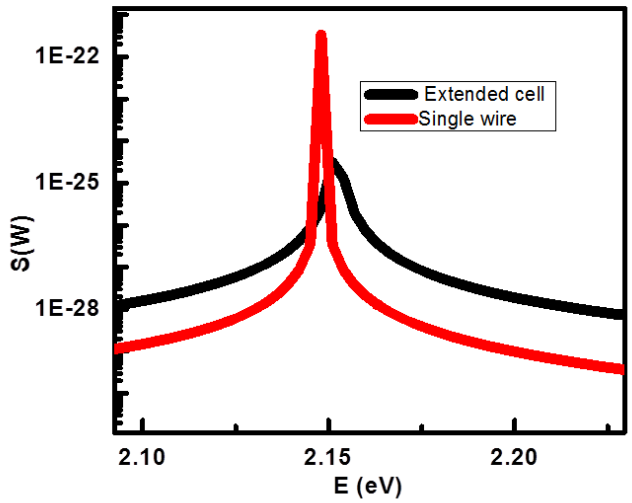

Figure S13: *S* (ω) for single dipole with different FDTD templates.

(d) **Effect of spacer layer thickness:**

In main manuscript Figure 3 (a) and (b) we have shown the S(ω) for three spcer layer thickness in 2D plot. In figure S14 we have shown the evolution of the S(ω) as a function of spacer layer thickness in 3D. In figure we are also shown the how the peak position changing with the "h" also shown with dotted line.

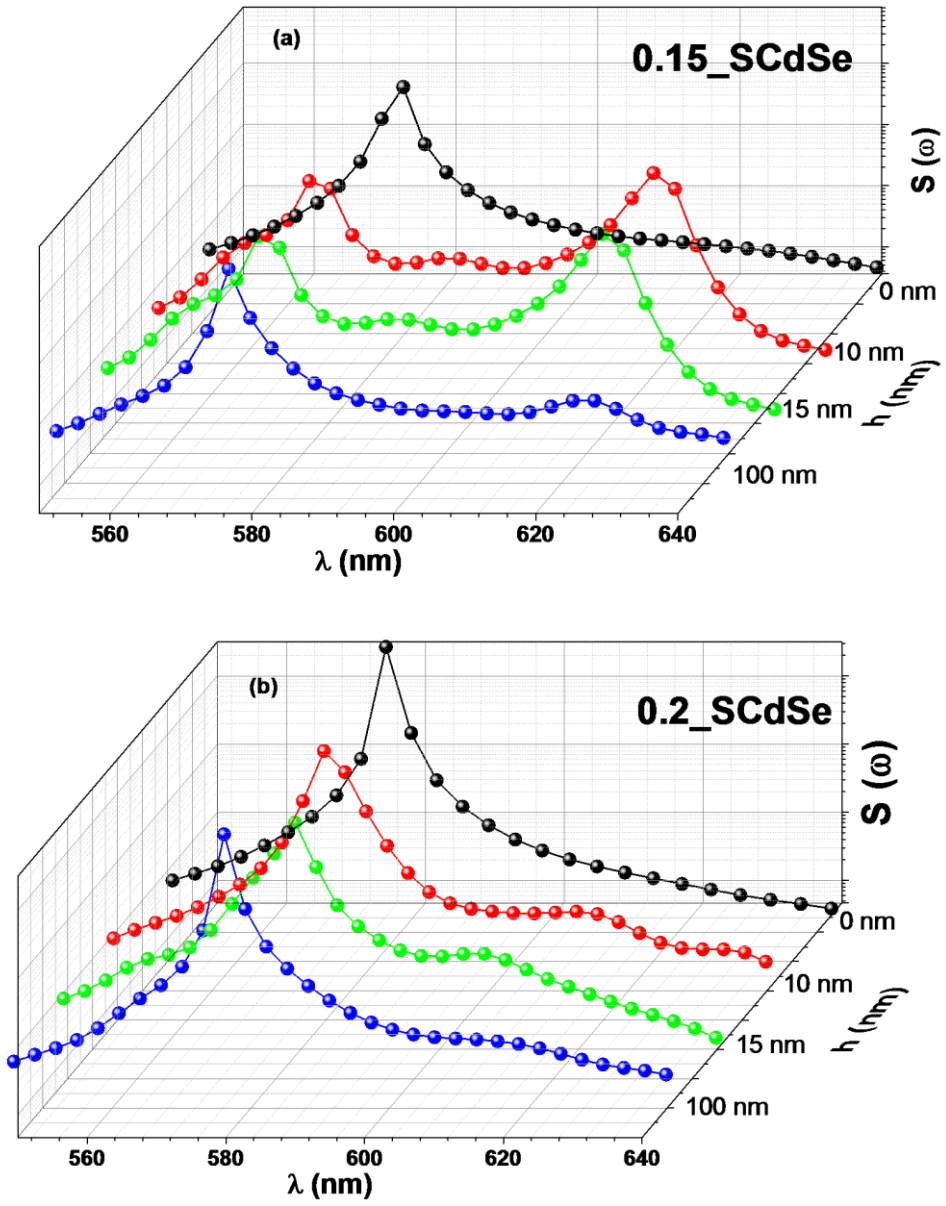

Figure 14: Shows the S(ω) as a function of spacer layer thickness for (a) 0.15 and (b) 0.2 filling fraction.

(d) LDOS and Calculation of coupling efficiency (β) between QDs and HMM modes:

Calculation of LDOS:

The dyadic Green's function *G* is defined as electric field at point, *"r"* , due to dipole having dipole moment μ aligned along z axis at spatial position r_0

$$G_{ZZ} = \frac{E_Z c^2 \epsilon_r \epsilon}{\omega^2 \mu} \quad (9)$$

The LDOS along z axis

$$\rho_{zz}(r_0, \omega) = \frac{6\omega}{\pi^2} \{Im\{Gzz(r_0, r_0, \omega)\}\} \quad (10)$$

And along x axis

$$\rho_{xx}(r_0, \omega) = \frac{6\omega}{\pi^2} \{Im\{Gxx(r_0, r_0, \omega)\}\} \quad (11)$$

Total LDOS (ρ)

$$\rho = \rho_{zz}(r_0, \omega)/3 + 2 * \rho_{xx}(r_0, \omega)/3 \quad (12)$$

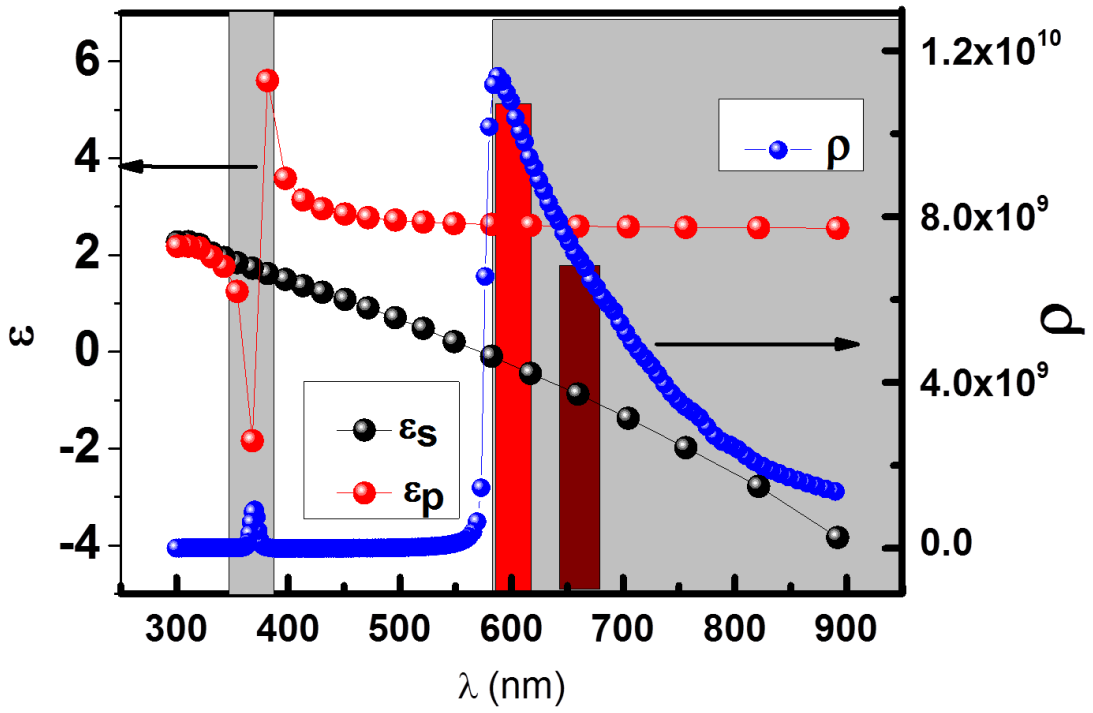

Figure S15: Shows the diagonal terms of the dielectric tensor as a function of the wavelength and corresponding LDOS as a function of wavelength. High K vector modes (hyperbolic region) shown in the shaded region. Regions indicated by the rectangles are the FWHM of the SCdSe and LCdSe QD'S.

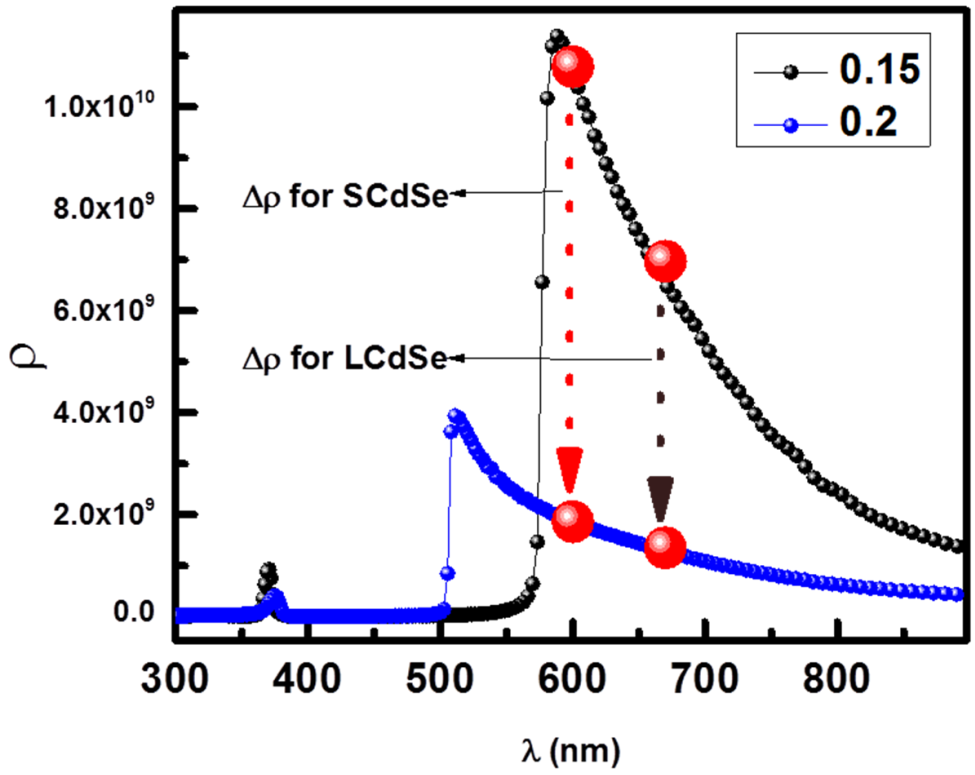

Figure S16: LDOS as a function of wavelength for f=0.15 and f=0.2 filling fraction and arrow shows the LDOS values corresponding to the SCdSe (dotted red line) and LCdSe (dotted gray line) for same spacer layer thickness.

Effect of filling fraction "f" on strong coupling:

As shown in figure S15, above, the cross over wavelength transition between dielectric dispersion to hyperbolic dispersion relation (topological transition) is changes. The LDOS of f=0.15 is very high compared to f=0.2 at same frequency which effects the coupling strength for different filling fractions. From figure S15 it is clear that due to shift in the LDOS positions in case of f=0.2 filling fraction the LDOS near QD frequency is reduced compared with the f=0.15 filling fraction samples with same spacer layer thickness. In figure we can see the change in the LDOS for both QD for f=0.15 and f=0.2.

Effect of "N" on strong coupling:

In case of super radiance mediated strong coupling the general splitting can be calculated using [9]

$$\Delta_E \approx \sqrt{{g_1}^2 * \frac{N}{3} - \frac{1}{16}\left(\gamma_{QD-}\ \gamma_{HMM}\right)^2}$$

Where "N" QD number in unit cell of the HMM and " γ_{QD} " and " γ_{HMM} " are decay rates of the QD and HMM templates. The " g_1 " is coupling strength from the collective dipole mode of the HMM template. We have neglected the additional factor coming from the higher multi modes which are responsible for the non radiative decay rates. These higher order modes acts like collective pseudo mode which is detuned from the QD emission. The " N/3" term coming from the number of degenerate dipoles collective modes.

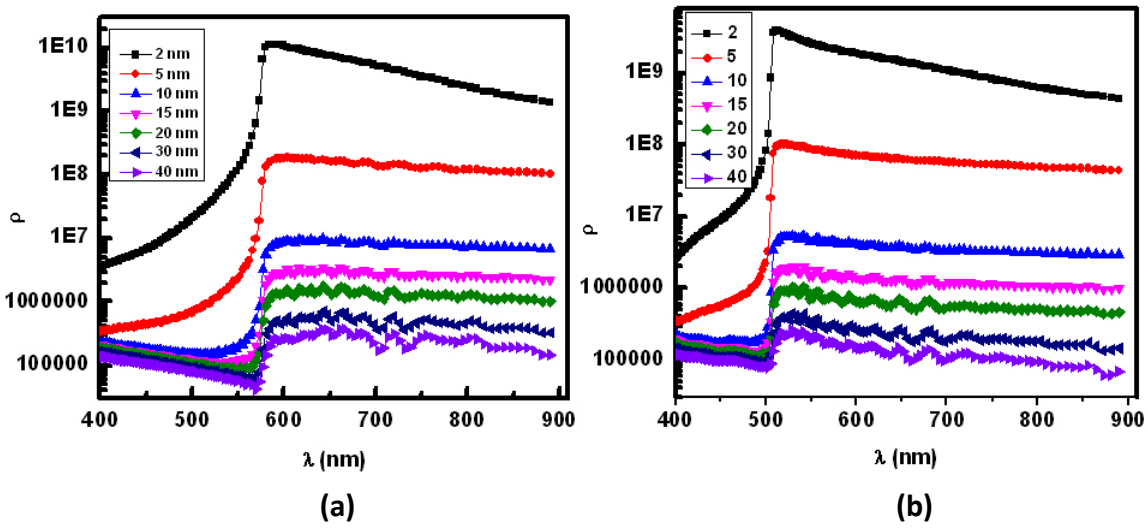

Figure S17: Distance dependent LDOS (ρ) as a function of wavelength for HMM templates with (a) *f*=0.15, (b) *f*=0.20 .

Figure S17 shows that the magnitude of ρ decreases with the increase in distance from the surface of HMM templates (*h*) and the cut-off frequency for enhancement of ρ is independent of the distance in both templates.

Calculation of β-factor:

We have observed non monotonic variation in the *S* (ω) as a function of *h*. To understand this non-monatomic variation in splitting, we have to calculate the distance dependent coupling strength between QD and high wave vector (high K vector) mode of HMM. β-factor gives the information of the coupling efficiency between QD and high wave vector of HMM. The β-factor is defined as

$$\beta = \frac{\Gamma_{HMM}}{(\Gamma_{rad} + \Gamma_{Nrad})} \quad (13)$$

$$\Gamma_{HMM} = \frac{3\pi\lambda}{4n_1^2} \frac{\Delta\rho^{2D}(r_0, K_{HMM})}{K_{HMM}.L_{HMM}} . \Gamma_0 \quad (14)$$

Here, Γ_0 is the decay rate of QD in free space and Γ_{HMM} is decay rate due to high wave vector vector mode

Γ_{HMM} = High K mode decay rate

K_{HMM} = collective mode wave vector

L_{HMM}: propagation length of HMM mode.

$$\Gamma_{tot} = \Gamma_{rad} + \Gamma_{Nrad}$$

$$\Gamma_{tot} = \frac{2\omega}{3h\varepsilon_0} |\mu|^2 \rho_z(r0, \omega) \quad \textbf{(15)}$$

Calculation of *β* factor for HMM template:

For calculating "*β* factor", we have to calculate two terms. One is decay rate of High K vector mode and total decay rate of dipole in HMM. From equation (11), it is clear that decay rate of high K vector mode is proportional to the LDOS and ($1/L_{HMM}$) . We calculated LDOS and fitted with Lorentzian shape to find $\Delta\rho^{2D}(r_0, K_{HMM})$ at K_{HMM} and FWHM which is proportional to ($1/L_{HMM}$). Free space decay rate is calculated by LDOS without HMM. Total decay rate of dipole in HMM is calculated using equation (12).To see the distance dependence, we calculated β factor by placing a dipole as a function of distance from the HMM templates following methods used for earlier studies [8]. Since we only concentrated on the distance dependence so we calculated normalized *β* factor with respect to value of *β* factor at 10 nm (where *β* is maximum).

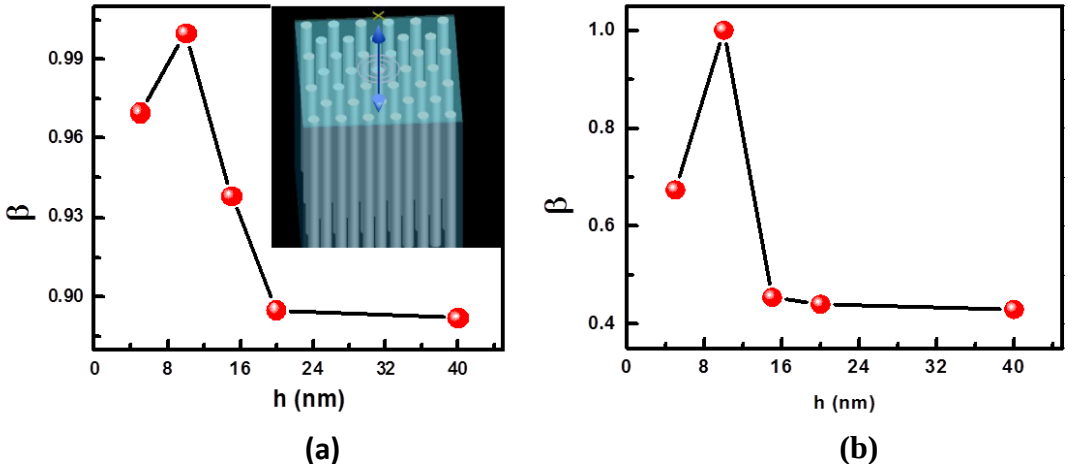

Figure S18: Calculated β-factor as a function of spacer layer thickness for SCdSe and HMM template with **(a)** *f*= 0.15 and **(b)** *f*=0.2. Inset in the **(a)** shows the schematic diagram of the template used in these calculations.

(e) ΔE_{FDTD} calculation: Now, to understand experimental results we have calculated splitting as a function of spacer layer thickness as defined in the main manuscript is product of the spectral density function *S(ω)* and *β*-factor. This is clear from the experimental results far field emission spectra are changing with the spacer layer thickness. The far field emission spectra has contribution from both propagating Greens function part of the *S(ω)* and coupling strength between a QD and HMM template (*β*-factor). In fact as can be seen from the β-factor calculations for both templates we find that very close to the template this quantity decreases which is indicative of the fact that non-radiative coupling, largely plasmonic in origin, starts dominating at such separations. Since the calculation of *S(ω)* does not take this non-montonic nature of coupling strength between QDs and HMM template into account hence to compare the experimental data ΔE_{exp} we have defined a new quantity, ΔE_{FDTD}, which is proportional to the product of these two factors (Eq. 2 in main manuscript). More accurate theoretical studies required to understand more quantitative significance of the analytical or numerical studies to match the experimental results in these systems. With this formalism, we can explain quantitatively the splitting and its dependence on the spacer layer thickness.

(5) Time resolved Photoluminescence (TRPL) measurements

In addition to steady state PL measurements we also performed TRPL measurements. All the time resolved photoluminescence measurements were performed with 469 nm diode laser with repetition rate 1MHz. The signal is collected in reflection mode and the detector placed normal to the sample. The PL signal passes through the monochromator, so all the TRPL measurements were performed on the single wavelength. We selected single wavelength corresponding to the PL peak position for all the measurements. The time resolved decay curves were fitted with multi exponential function of the form shown below in Eqn. (1).

$$\boldsymbol{I = a1 * e^{\frac{t1}{\tau}} + a2 * e^{\frac{t2}{\tau}}} \qquad (16)$$

Here t1, t2, are the respective decay times and *a*1, *a*2, are the corresponding normalized amplitudes, respectively. Example of fit to a typical TRPL data is shown in **Figure S16**.

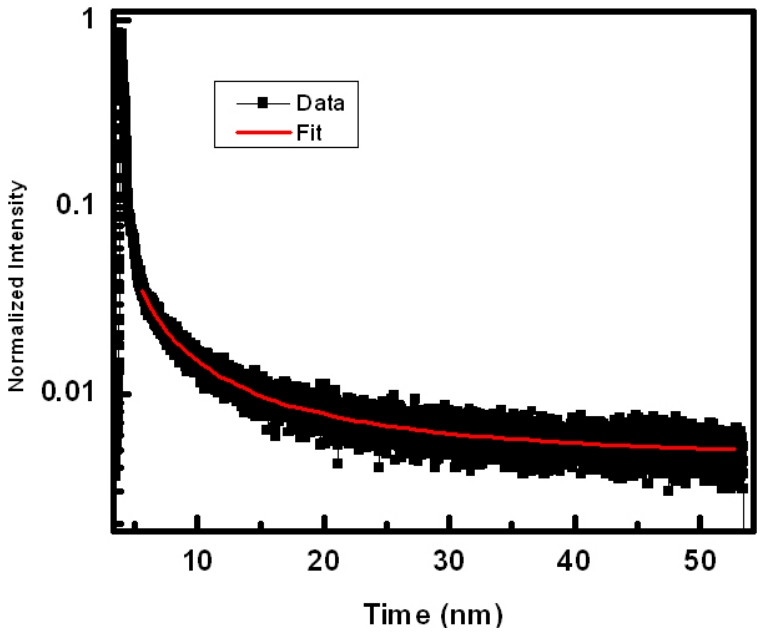

Figure S19: Shows the typical TRPL spectra (symbol) and corresponding fit (solid line) using equation 16**.**

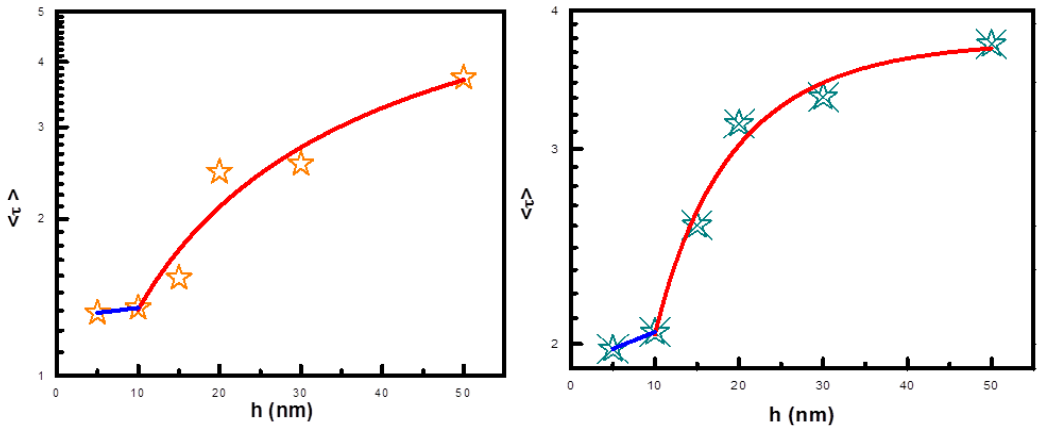

(a) **(b)**

Figure S20: Shows the typical average decay times as a function of *h* for HMM template with **(a)** *f*= 0.15 and **(b)** *f*=0.20. Figure shows experimental data (symbol) and corresponding fit (exponential function: red line) for h >10 nm and for h < 10 (Power law: blue line).

The average life time is calculated using equation (15) .

$$< \tau >= \frac{\sum a_i * \tau_i^2}{\sum a_i * \tau_i} \qquad (17)$$

The average life time as a function of spacer layer thickness *h* displays two regimes of variation of life time as shown in **figure S20** .

Figure S21 shows the LDOS as a function of " *h*" at wavelength corresponding to the PL peak positions of the LCdSe and SCdSe QDs. From the figure it is clear that we observed two different regions of distance dependence. In one region ρ has power law dependence while in the other region it shows exponential dependence. This distance dependence of LDOS is independent of *f* and indicates the generic nature of HMMs. The exponential decay of LDOS with distance attributed to the plasmonic decay rate of the template and power law dependence on the distance is due to high wavevector components of HMM. This also clear that power law dependence is coming at very short distance due to near field interaction between QDs and high K modes of the HMM templates. What is also clear is the larger LDOS for *f* = 0.15 template over the *f* = 0.2 template as well as larger LDOS for SCdSe compared to LCdSe. This also explains the larger g(h) in FDTD and ΔE_{exp} observed in experiments for *f* = 0.15 over *f* = 0.2 and SCdSe over LCdSe QDs for a given HMM template.

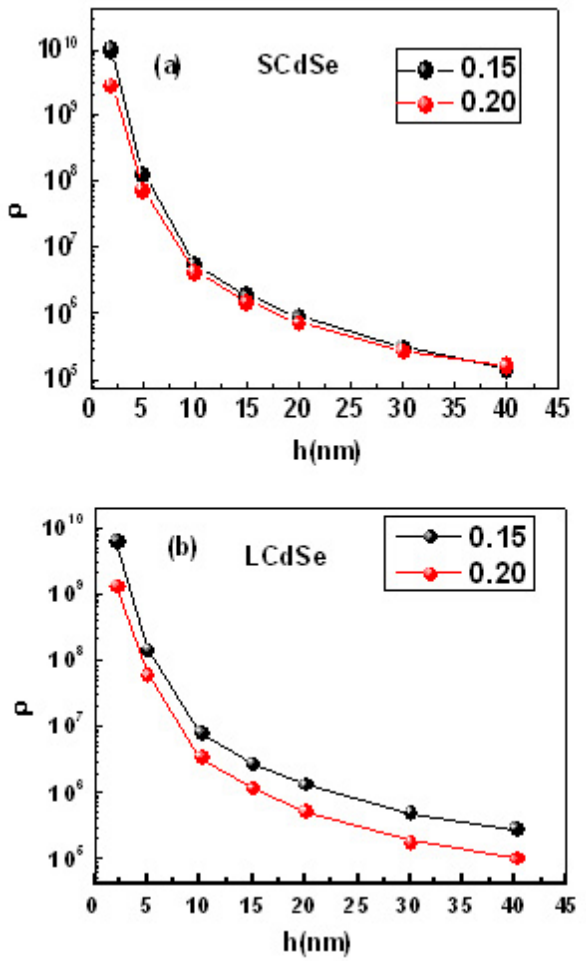

Figure S21: shows comparison of LDOS (ρ) as a function of spacer thickness for both HMM templates with **(a)** SCdSe , **(b)** LCdSe.

By effective medium theory, we calculated the LDOS as function of spacer thickness (h) and explained the observed changes in the decay dynamics and PL intensity quenching as a function of *"h"*. In fact this also additional evidence which indicates that the existence of non-monotonic variation of ΔE_{exp} is due to two different modes which couple to the QDs and the next effect observed in experiments can be explained by combining the coupling efficiency and the spectral density function.

Reference:

1) Jyotirmayee Kanungo. and Joerg Schilling "Experimental determination of the principal dielectric functions in silver nanowire metamaterials Appl.Phy.Lett 97, 021903. (2010).
2) Z. A. Peng and. X. Peng "Formation of high-quality CdTe, CdSe, and CdS nanocrystals using CdO as precursor. " J. Am. Chem. Soc., 123, 183. (2001).
3) M. Haridas, L. N. Tripathi. and J.K. Basu. " Photoluminescence enhancement and quenching in metal-semiconductor quantum dot hybrid arrays " Applied. Physics. Letter, 98, 063305. (2011).
4) L.N. Tripathi, M Praveena , Pranay Valson , J.K.Basu. "Plasmonic Tuning of Photoluminescence from Semiconducting Quantum Dot Assemblies" Applied.Physics.Letter, , 105, 163106. (2014).
5) Lorenzo Ferrari, Chihhui Wu , Dominic Lepage , Xiang Zhang . " Hyperbolic metamaterials and their applications "Progress in Quantum Electronics, , 40, 1–40. (2015).
6) C. Van Vlack, Philip Trst Kristensen , and S. Hughes . "Spontaneous Emission Spectra and Quantum Light-Matter Interactions from a Strongly-Coupled Quantum Dot Metal-Nanoparticle System " Phy.Rev B 85,076533. (2012).
7) P.B Johnson. and.R.W. Christy " Optical Constants of the Noble Metals "Phy.Rev.B,6,12. (1972).
8) Julien Barthes, Alexandre Bouhelier, Alain Dereux & Ge´rard Colas des Francs," Coupling of a dipolar emitter into one-dimensional surface plasmon" SCIENTIFIC REPORTS, 3 , 2734 doi: 10.1038/srep02734(2013).
9) A. Delga, J. Feist, J Abad-Bravo, J.F. Garcia-Vidal. Phy.Rev.Lett 112 253601,(2014).